OBRATOVALNA TRDNOST

Predloge k predavanjem

1. del

Nagode Marko

Univerza v Ljubljani, Fakulteta za strojništvo
Aškerčeva 6, SI-1000 Ljubljana, Slovenija

2012

Poškodbe kristalne rešetke

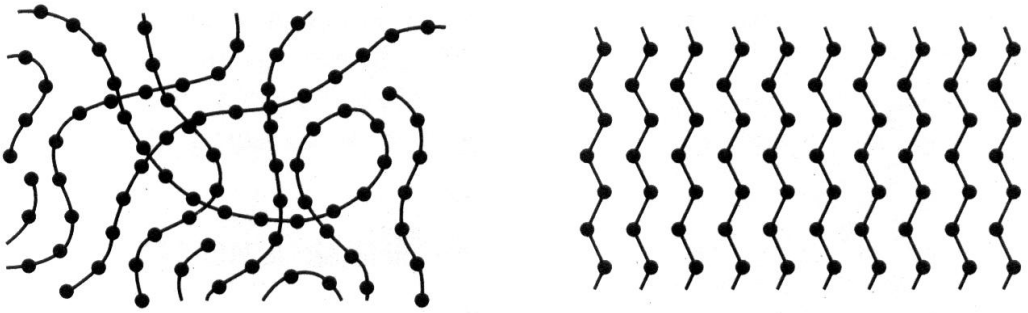

Figure 2.11 Two-dimensional schematics of amorphous structure (left) and crystalline structure (right) in a polymer.

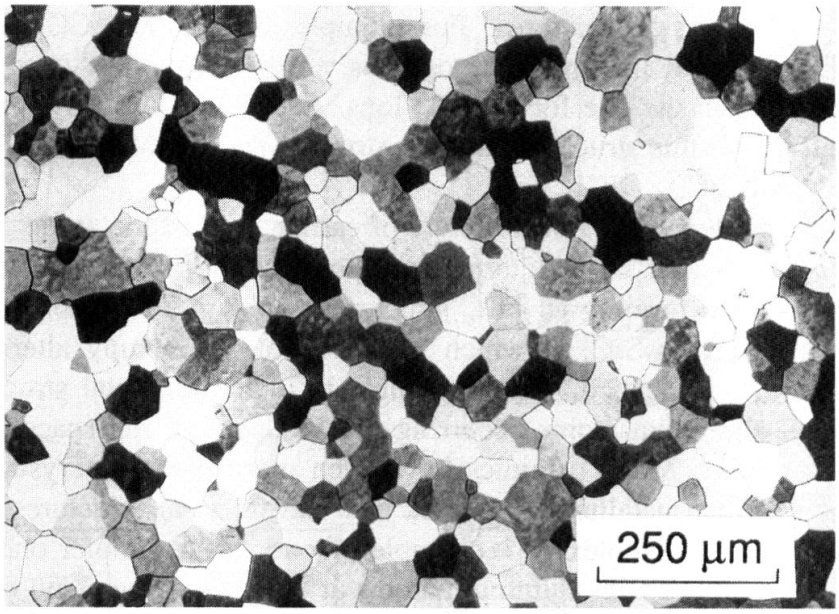

Figure 2.12 Crystal grain structure in the alpha form of the alloy Ti-6Al, which is titanium with 6% aluminum. (Photo courtesy of C. G Rhodes, Rockwell International Science Center, Thousand Oaks, CA.)

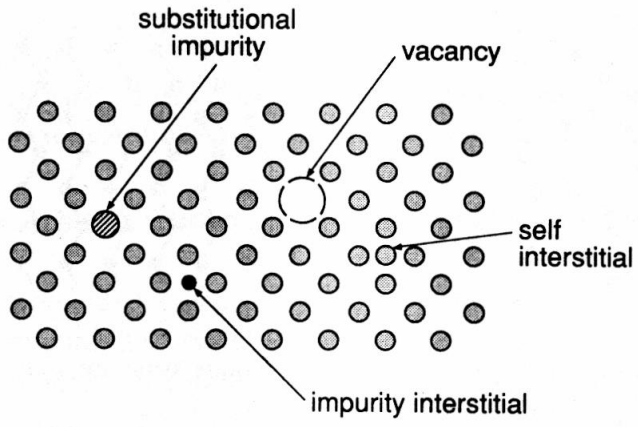

Figure 2.13 Four types of point defect in a crystalline solid.

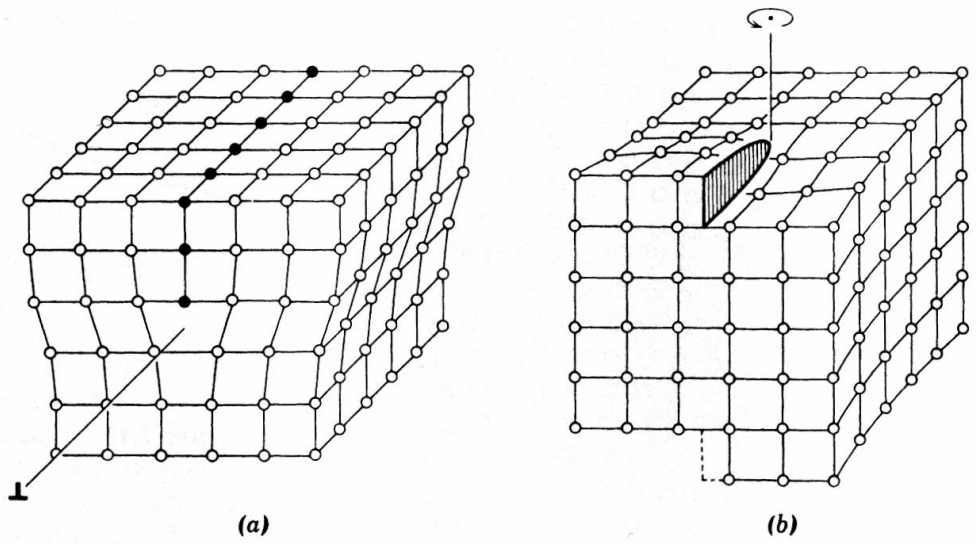

Figure 2.14 The two basic types of dislocations: (a) edge dislocation, and (b) screw dislocation. (From [Hayden 65] p. 63; used with permission.)

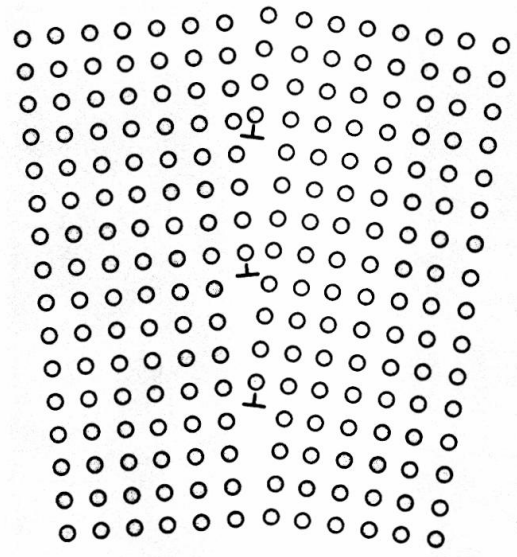

Figure 2.15 Low-angle boundary in a crystal formed by an array of edge dislocations. (From [Boyer 85] p. 2.15; used with permission.)

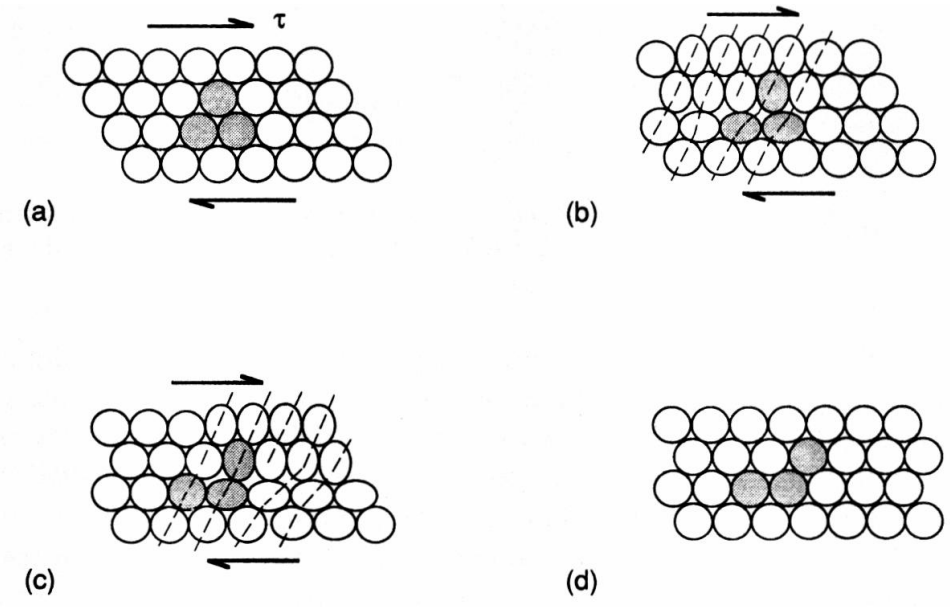

Figure 2.19 Shear deformation occurring in an incremental manner due to dislocation motion. (Adapted from *Elements of Materials Science and Engineering*, 6th Edition, by Lawrence Van Vlack; copyright ©1989, by Addison-Wesley Publishing Company; [Van Vlack 89] p. 265; reprinted by permission.)

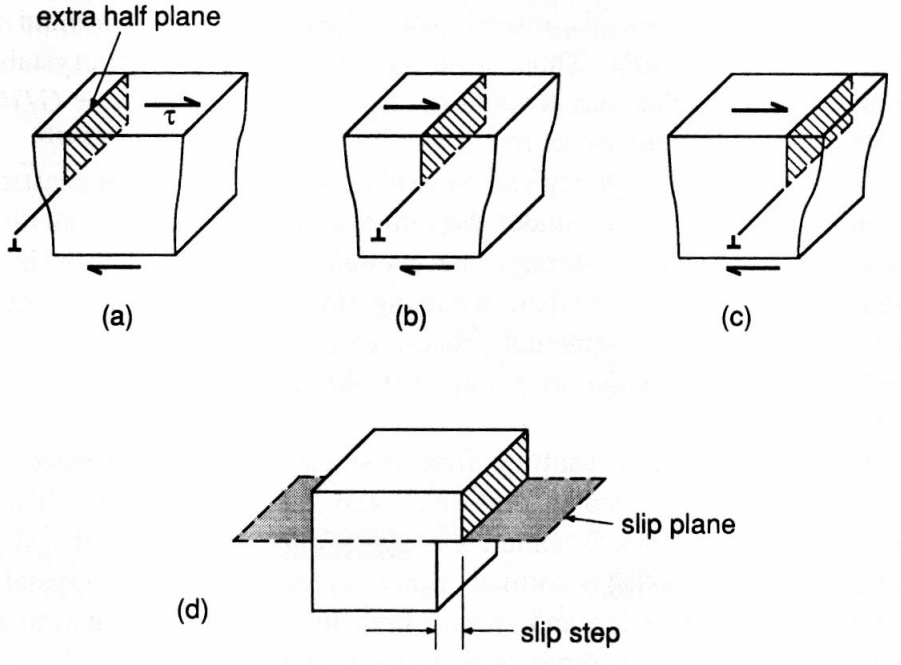

Figure 2.20 Slip caused by the motion of an edge dislocation.

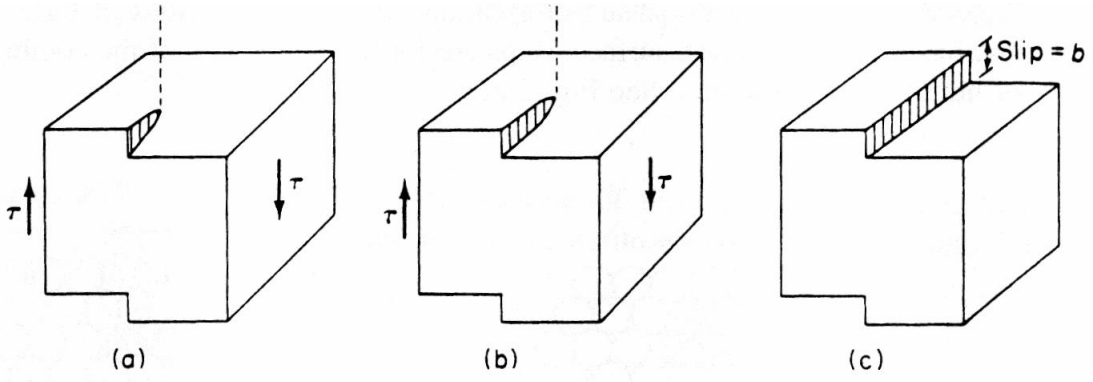

Figure 2.21 Slip caused by the motion of a screw dislocation. (From [Felbeck 96] p. 114; ©1996 by Prentice Hall, Upper Saddle River, NJ; reprinted with permission.)

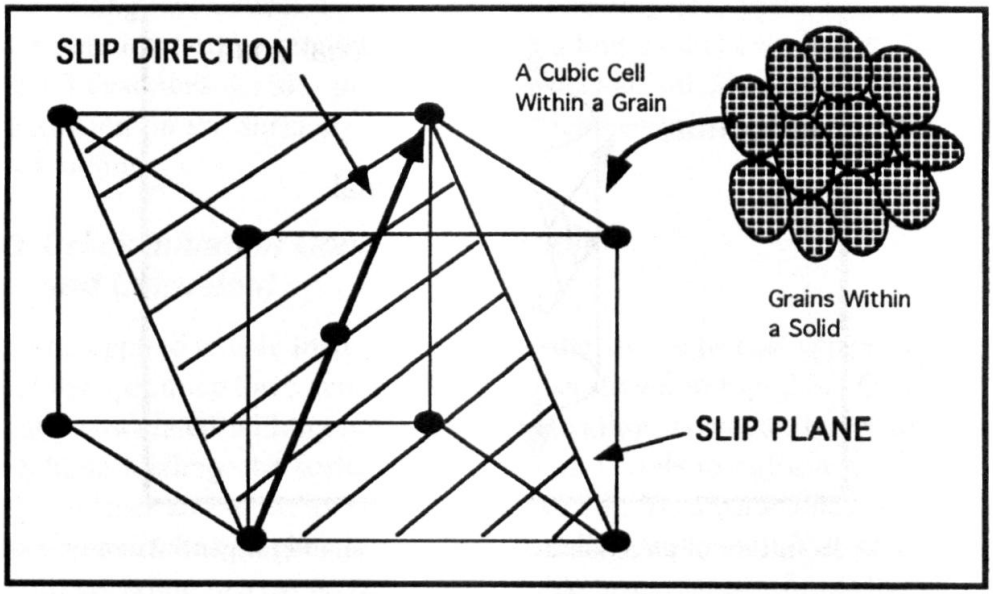

Figure 2.29 Illustration of slip plane and slip direction of a body centered cubic cell

Poškodbe zaradi monotone obremenitve

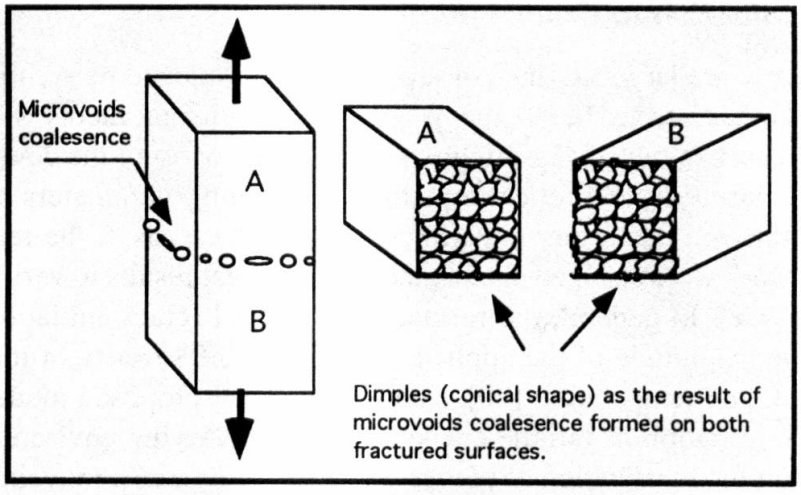

Figure 2.27a Microvoids coalescence and the formation of equiaxed dimples for tension overload.

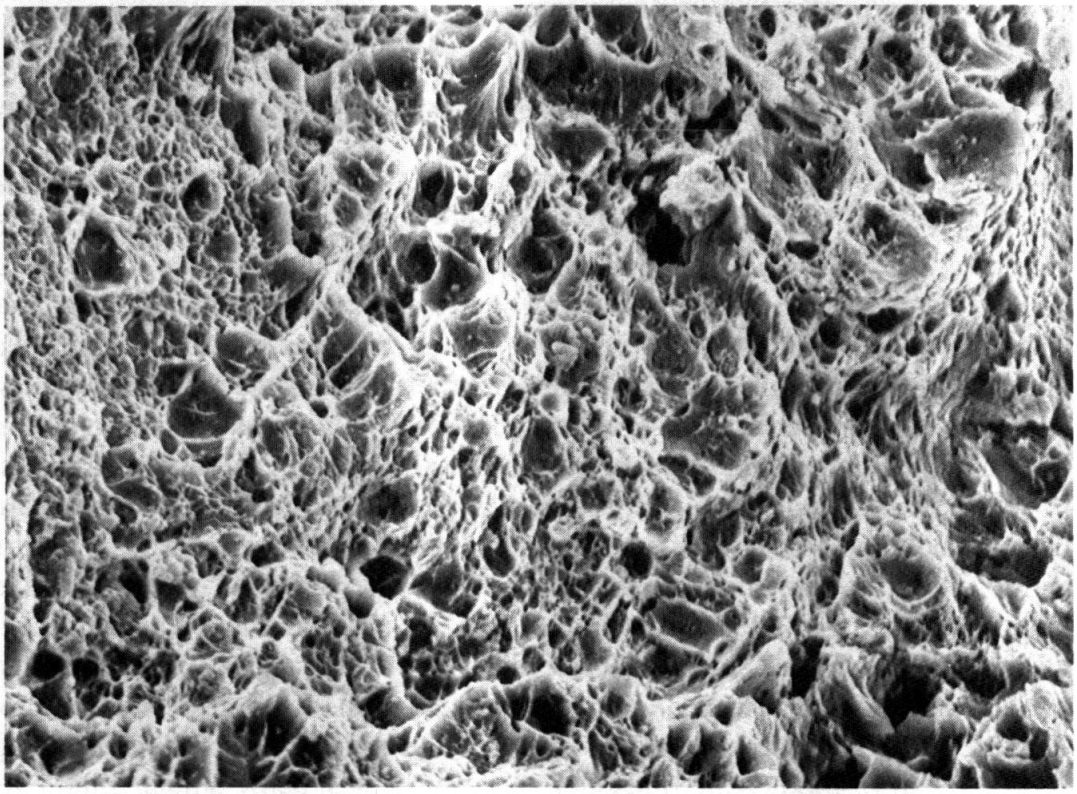

Figure 2.27b Formation of dimples for tension overload provided by the electron microscope (4340 steel with 180/200 ksi)

Poškodbe zaradi ciklične obremenitve

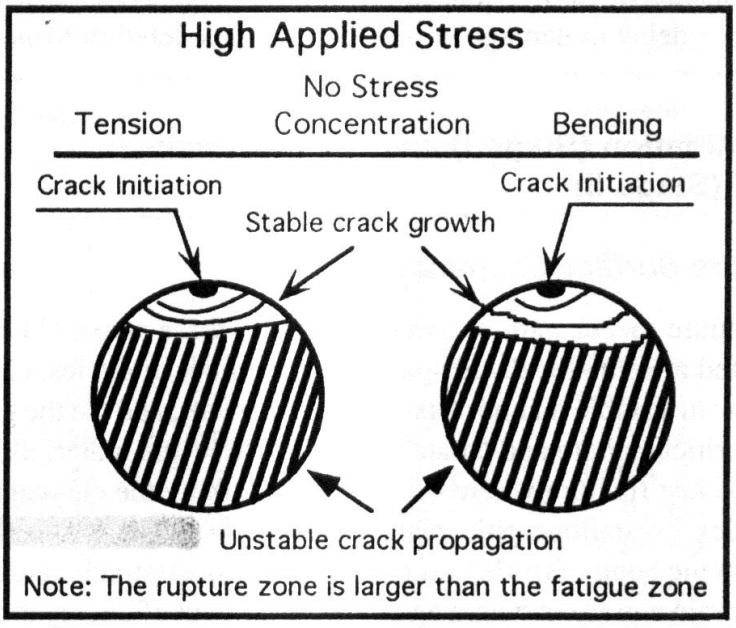

Figure 2.23 Generation of beach marks due to tension–tension and reversed bending high load for unnotched specimen

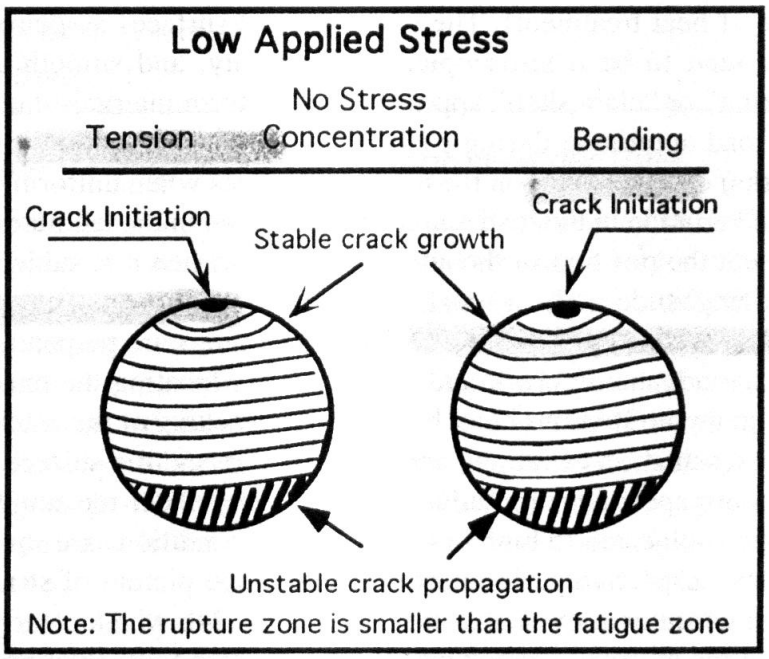

Figure 2.24a Generation of beach marks due to tension–tension and reversed bending low load for unnotched specimen

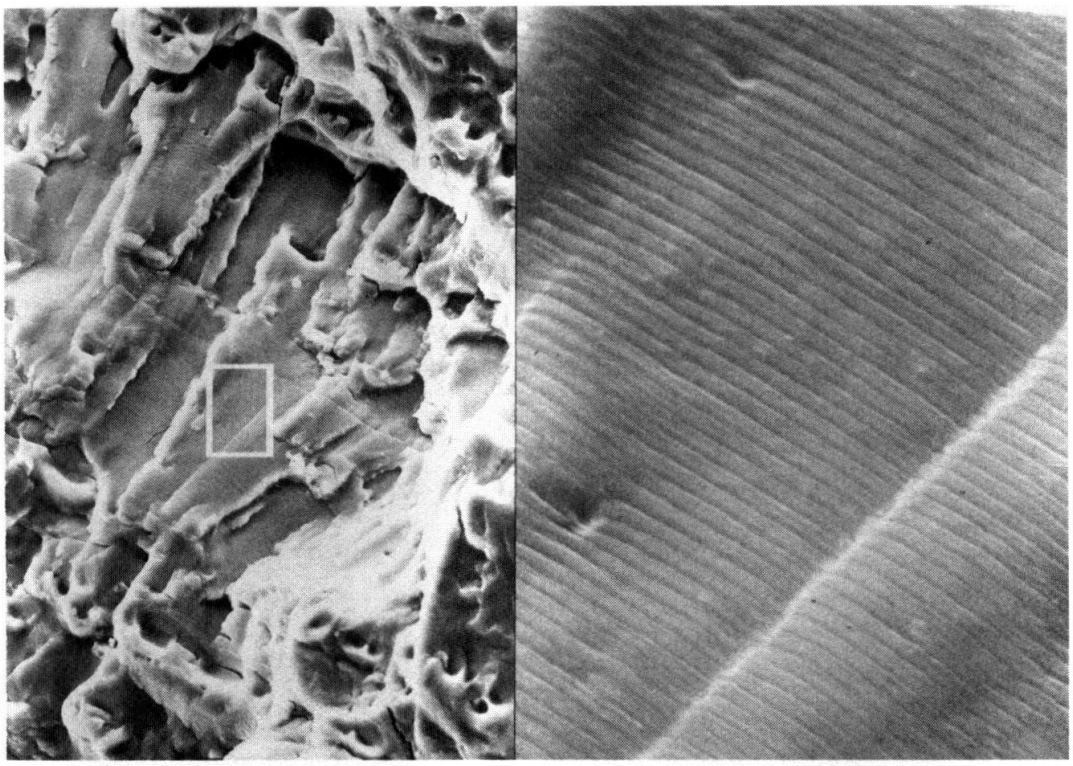

Figure 2.24b The striations marks provided by the electon microscopic technique for 6061-T6 aluminum alloy which represents the position of the advancing crack

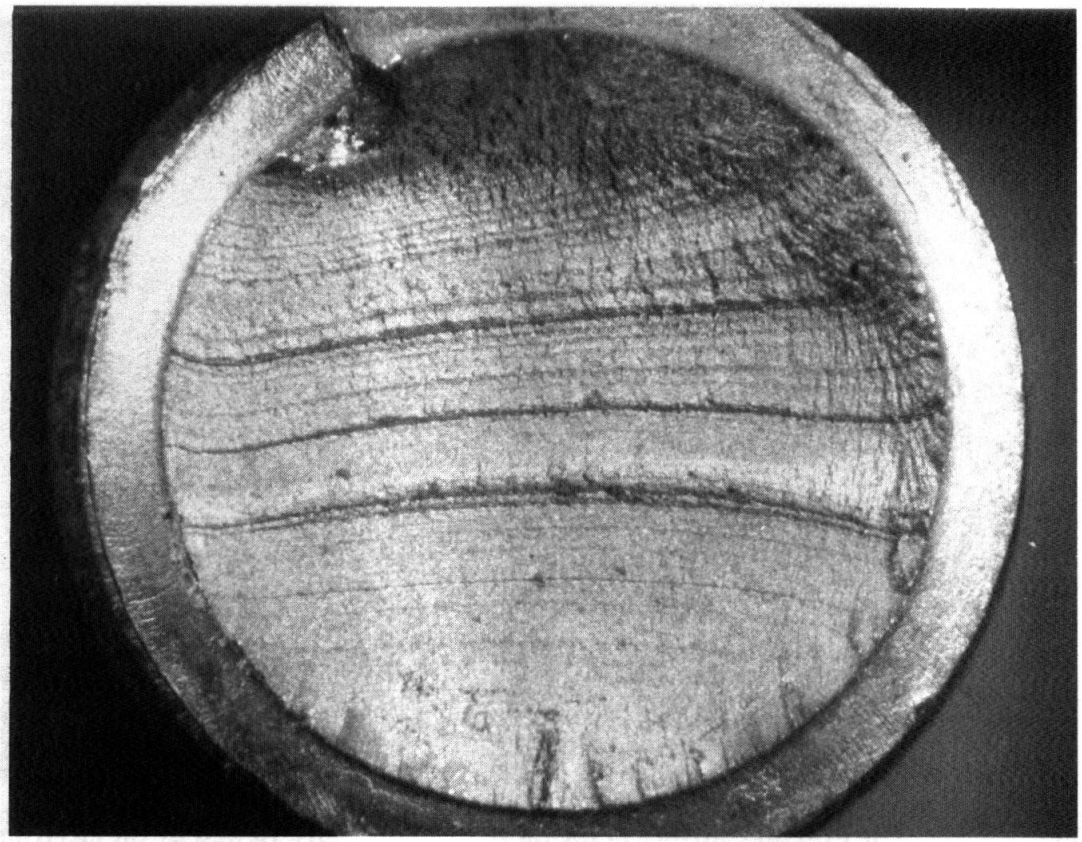

Figure 2.26 Fracture surface of a 4130 steel bolt viewed by a light microscope with a magnification factor of 16 × (striation marks on the fatigue zone can be seen on the surface of the part.)

Proces rasti utrujenostnih poškodb

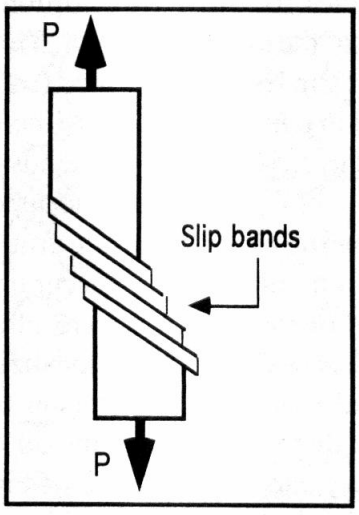

Figure 2.32 Illustration of slip by a monotonic tensile load

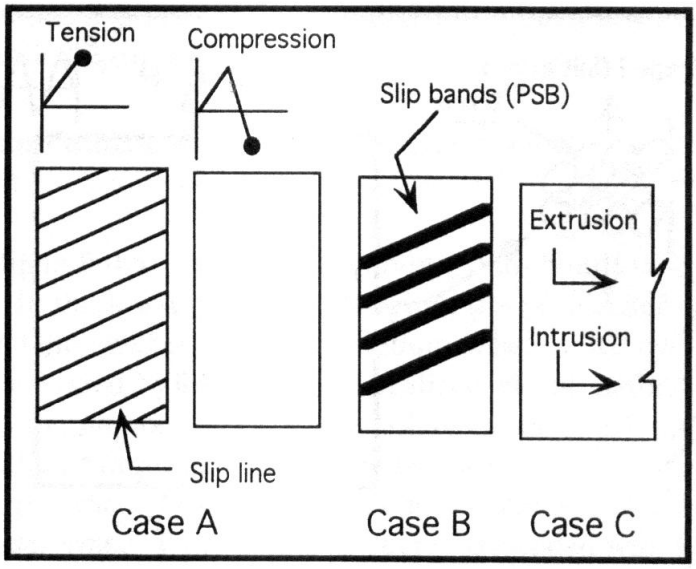

Figure 2.34 Slip lines and slip bands leading to crack initiation

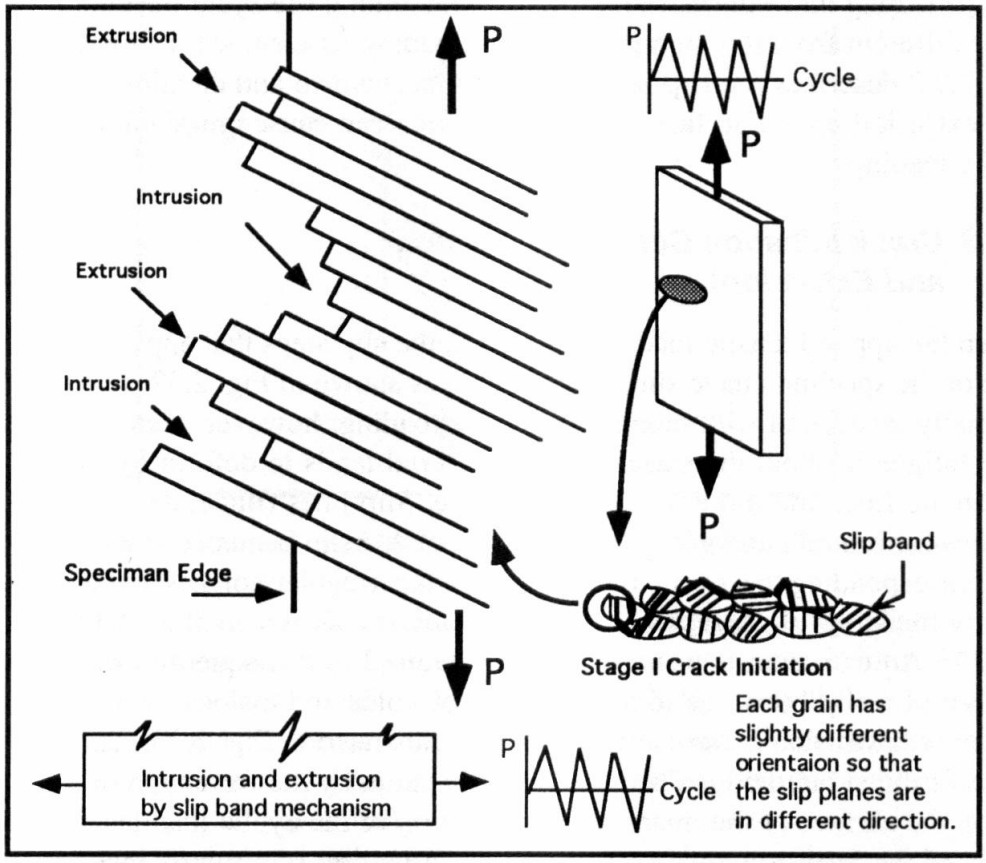

Figure 2.33 Illustration of intrusion and extrusion due to slip as a result of cyclic loading

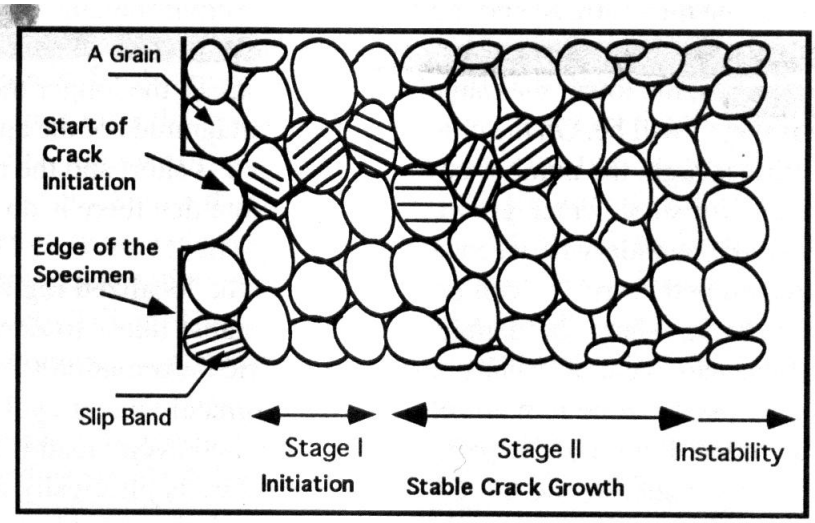

Figure 2.35 Illustration of stage I and stage II crack initiation and propagation

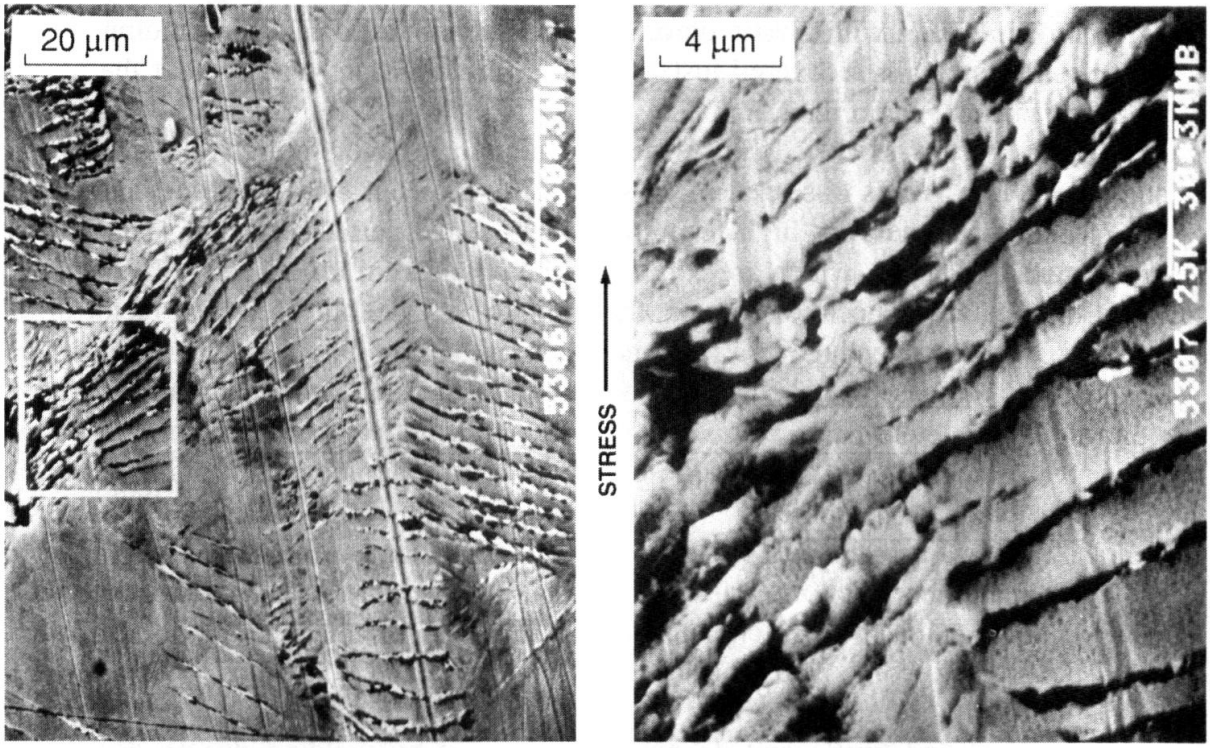

Figure 2.22 Slip bands and slip steps caused by the motion of many dislocations resulting from cyclic loading of AISI 1010 steel. (Photos courtesy of R. W. Landgraf, Virginia Tech, Blacksburg, VA.)

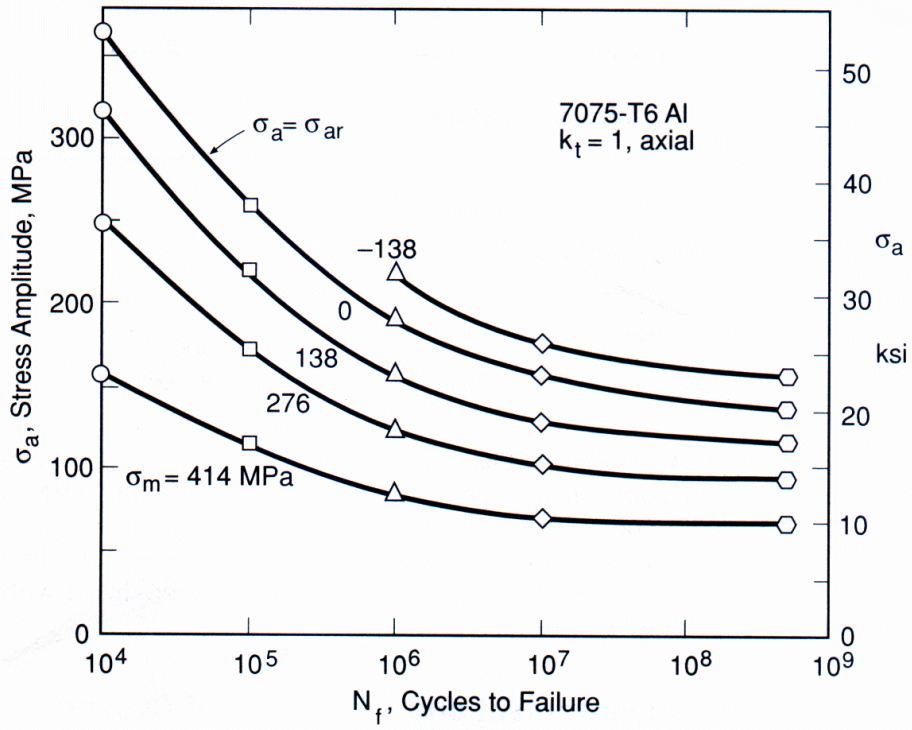

Figure 9.25 Axial loading *S-N* curves at various mean stresses for unnotched specimens of an aluminum alloy. The curves connect average fatigue strengths for a number of lots of material. (Data from [Howell 55].)

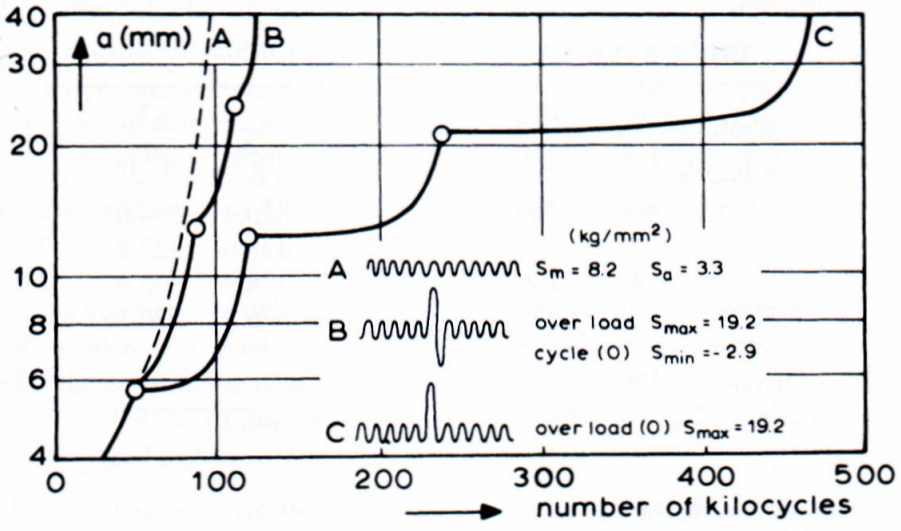

Figure 11.28 Effect of overloads on crack growth in center-cracked plates ($b = 80$, $t = 2$ mm) of 2024-T3 aluminum. (From [Broek 86] p. 273, as based on data in [Schijve 62]; reprinted by permission of Kluwer Academic Publishers.)

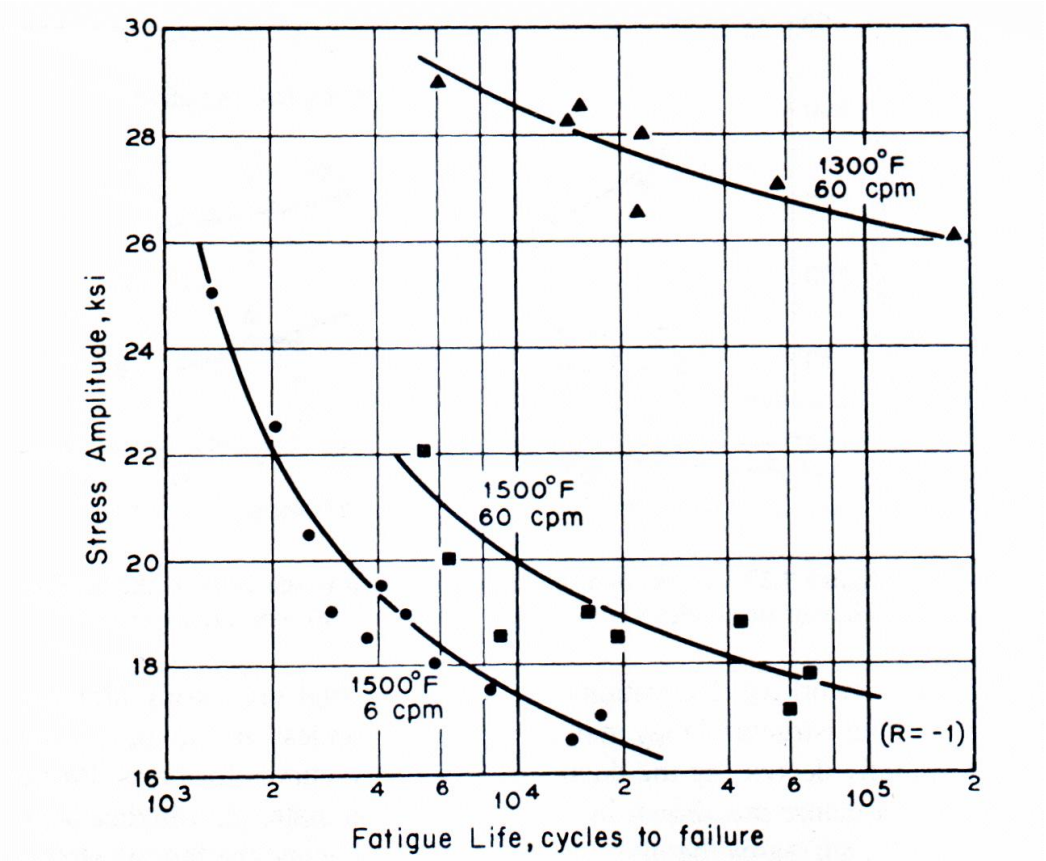

Figure 9.28 Temperature and frequency effects on axial *S-N* curves for the nickel-base alloy Inconel. (Illustration from [Gohn 64] of data in [Carlson 59]; used with permission.)

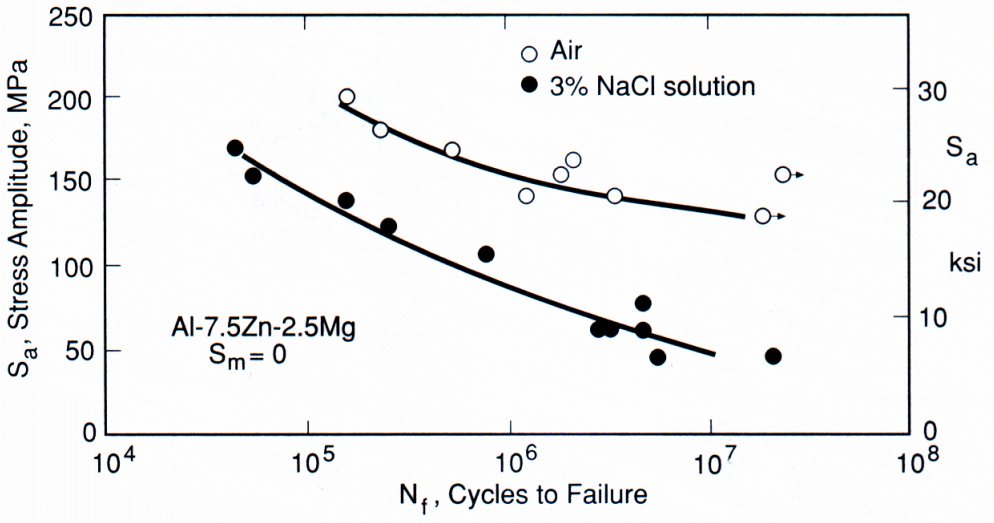

Figure 9.27 Effect of a salt solution similar to seawater on the bending fatigue behavior of an aluminum alloy. (Data from [Stubbington 61].)

Časovne zgodovine obremenitev

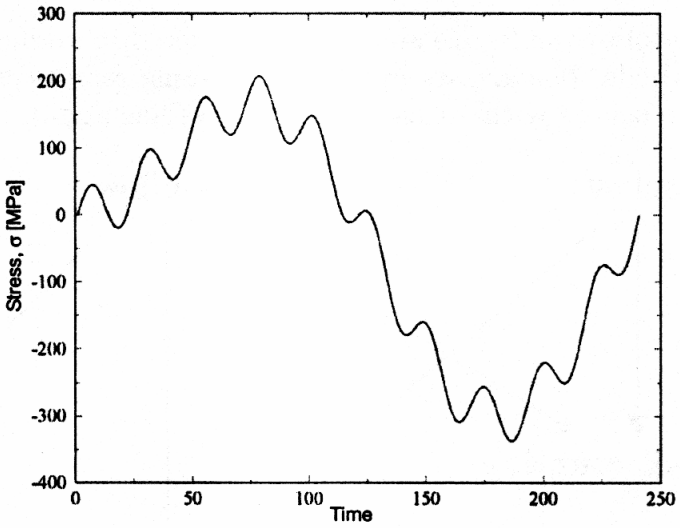

Fig. 11: Stress-time history.

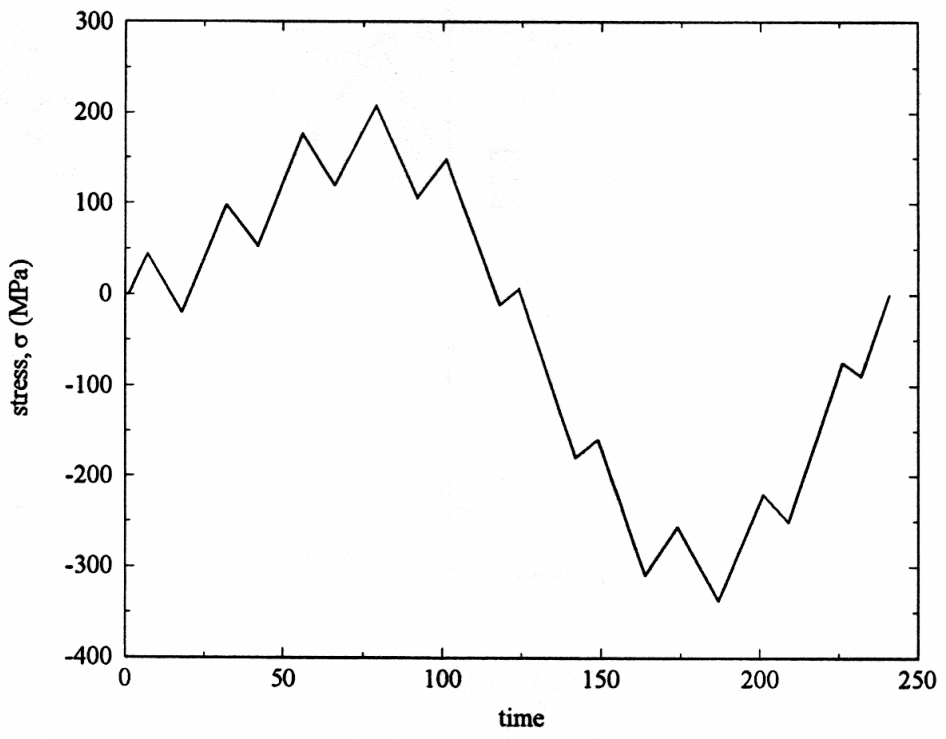

Fig. 12: Peak-picked stress-time history.

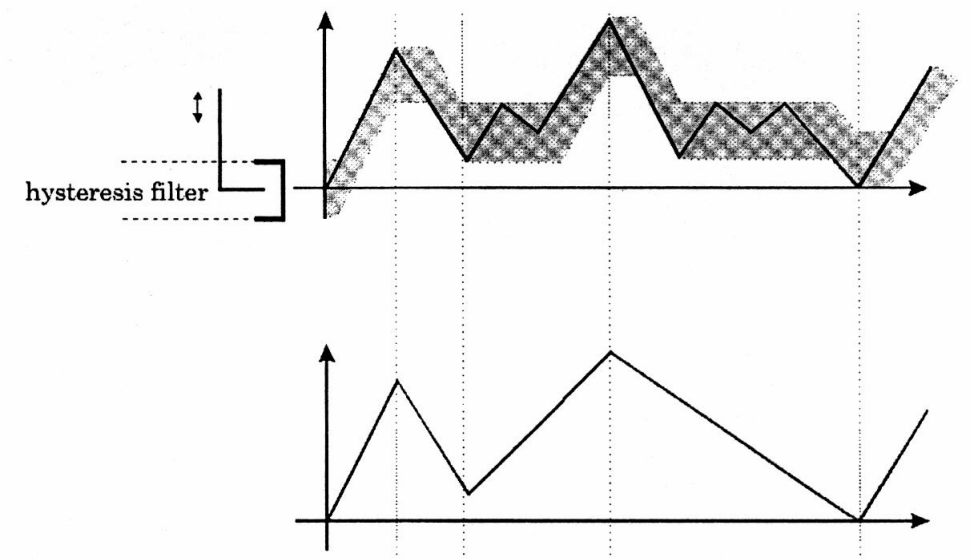

Fig. 13: Hysteresis filter

Značilni parametri časovnih zgodovin obremenitev

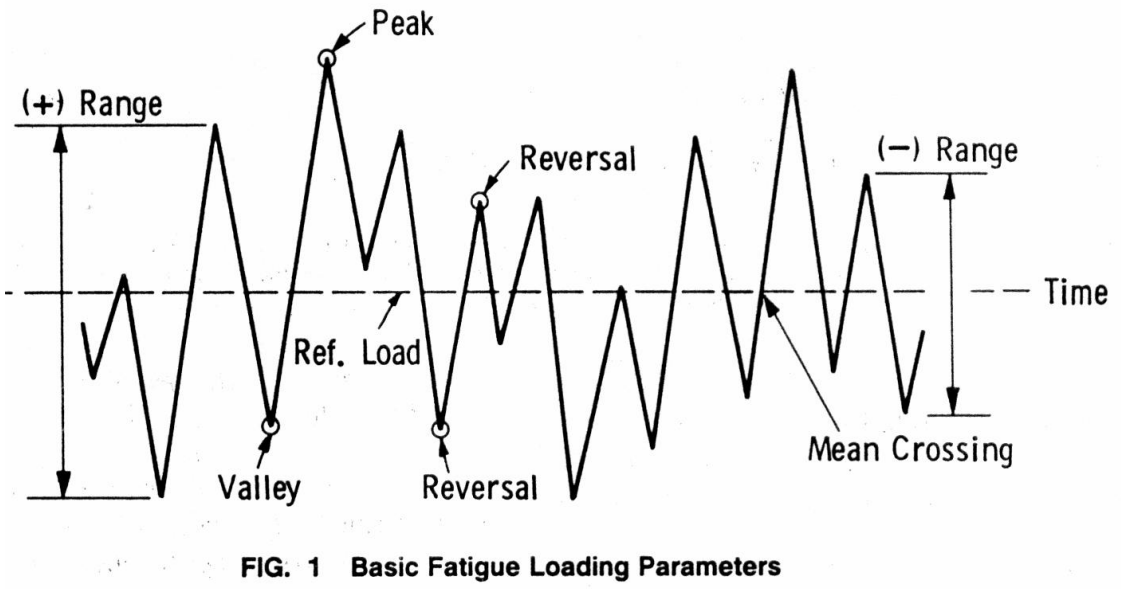

FIG. 1 Basic Fatigue Loading Parameters

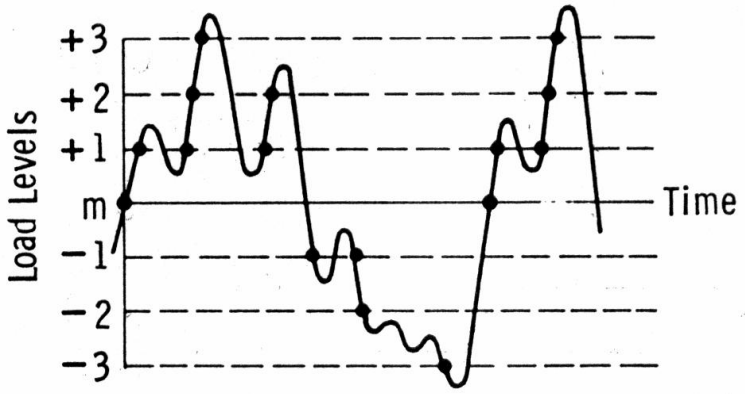

Level	Counts
+3	2
+2	3
+1	5
0	2
−1	2
−2	1
−3	1

(*a*)—Level Crossing Counting

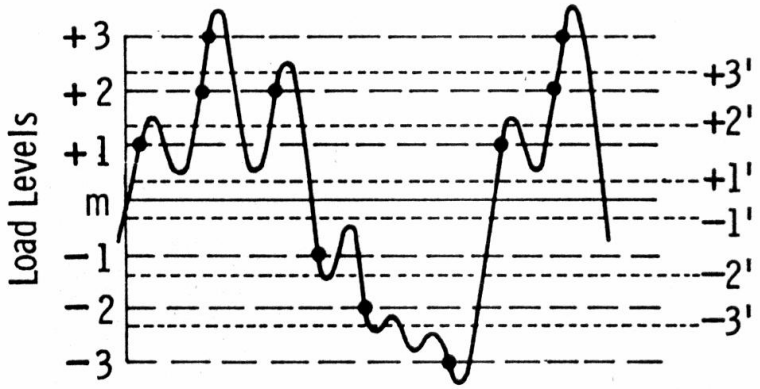

Level	Counts
+3	2
+2	3
+1	2
0	0
−1	1
−2	1
−3	1

(*b*)—Restricted Level Crossing Counting

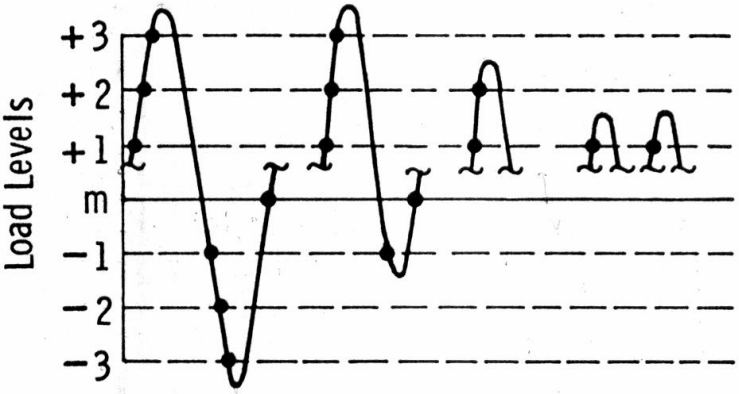

Range (levels)	Cycle Counts
7	1
6	0
5	1
4	0
3	0
2	1
1	2

(*c*)—Cycles Derived from Level Crossing Count of (*a*)

FIG. 2 Level-Crossing Counting Example

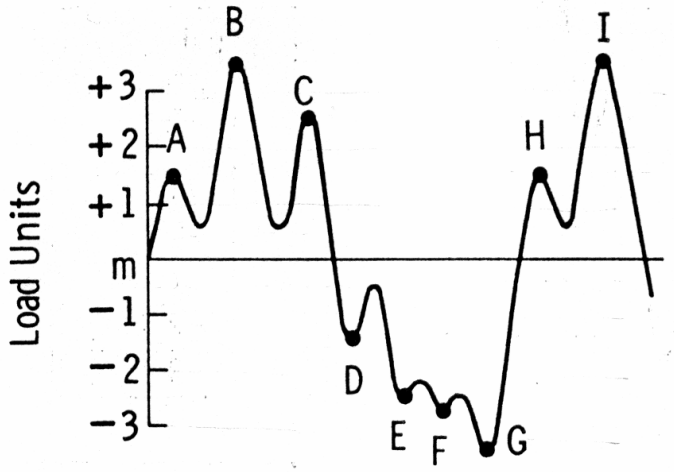

Peak	Counts
+3.5	2
+2.5	1
+1.5	2
−1.5	1
−2.5	1
−2.7	1
−3.5	1

(*a*)—Peak Counting

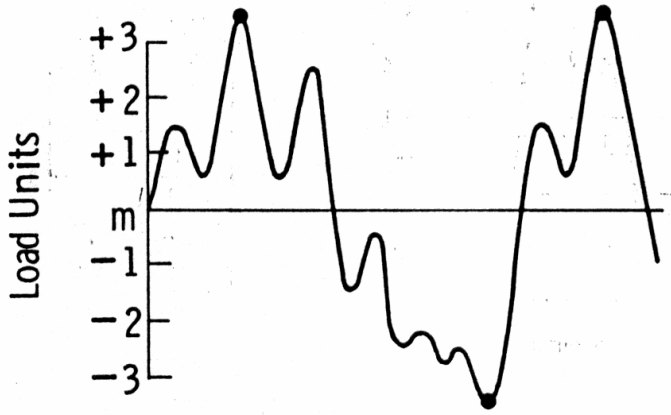

Peak	Counts
+3.5	2
−3.5	1

(*b*)—Mean Crossing Peak Counting

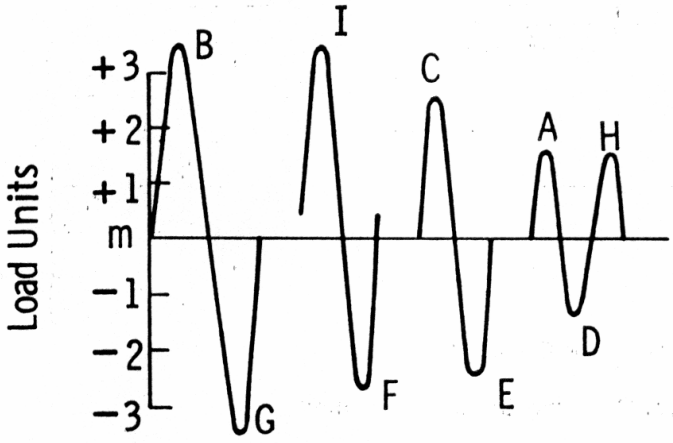

Range (units)	Cycle Counts
7	1
6.2	1
5	1
3	1.5

(*c*)—Cycles Derived from Peak Count of (*a*)

FIG. 3 Peak Counting Example

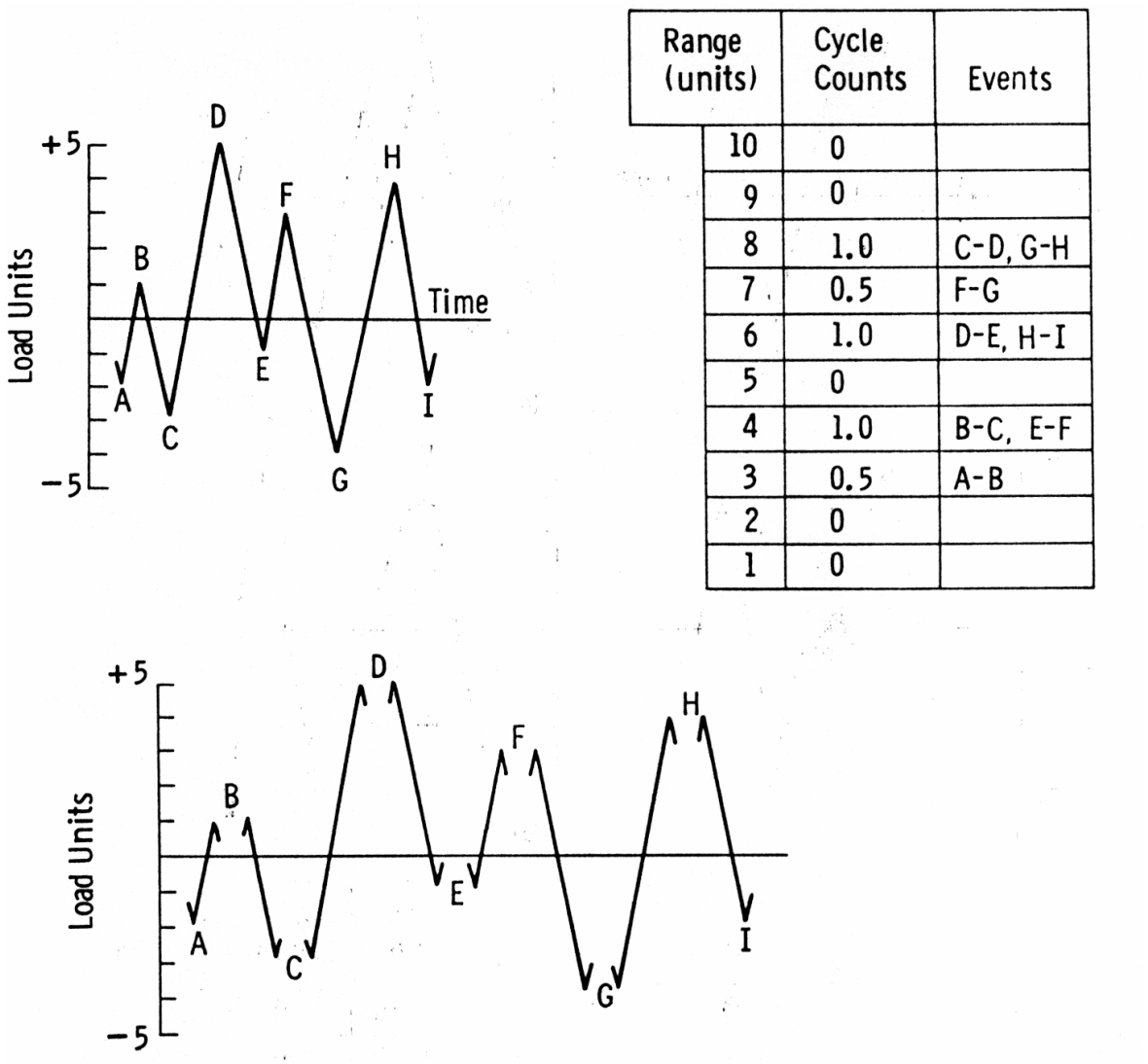

Range (units)	Cycle Counts	Events
10	0	
9	0	
8	1.0	C-D, G-H
7	0.5	F-G
6	1.0	D-E, H-I
5	0	
4	1.0	B-C, E-F
3	0.5	A-B
2	0	
1	0	

FIG. 4 Simple Range Counting Example—Both Positive and Negative Ranges Counted

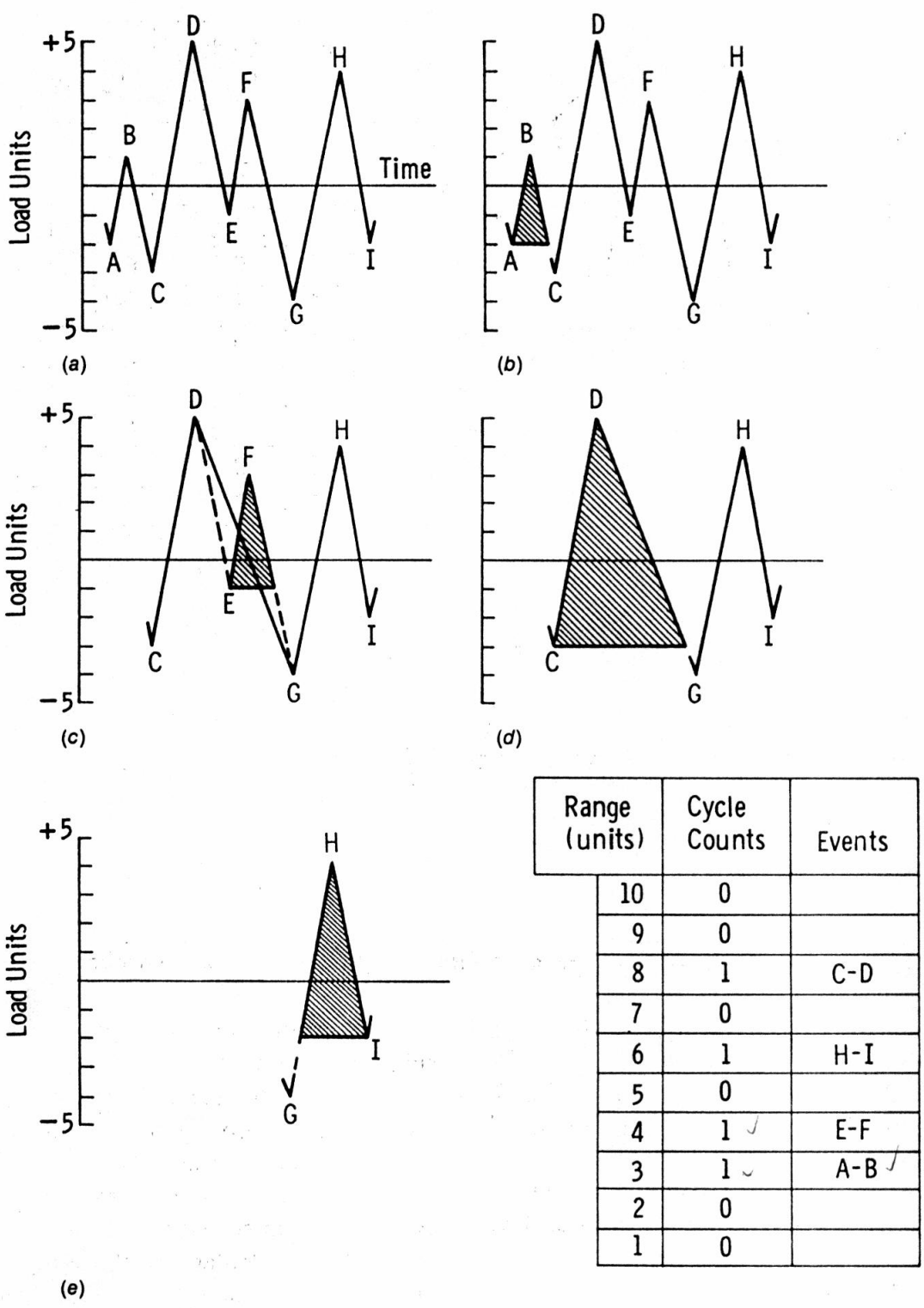

Range (units)	Cycle Counts	Events
10	0	
9	0	
8	1	C-D
7	0	
6	1	H-I
5	0	
4	1	E-F
3	1	A-B
2	0	
1	0	

FIG. 5 Range-Pair Counting Example

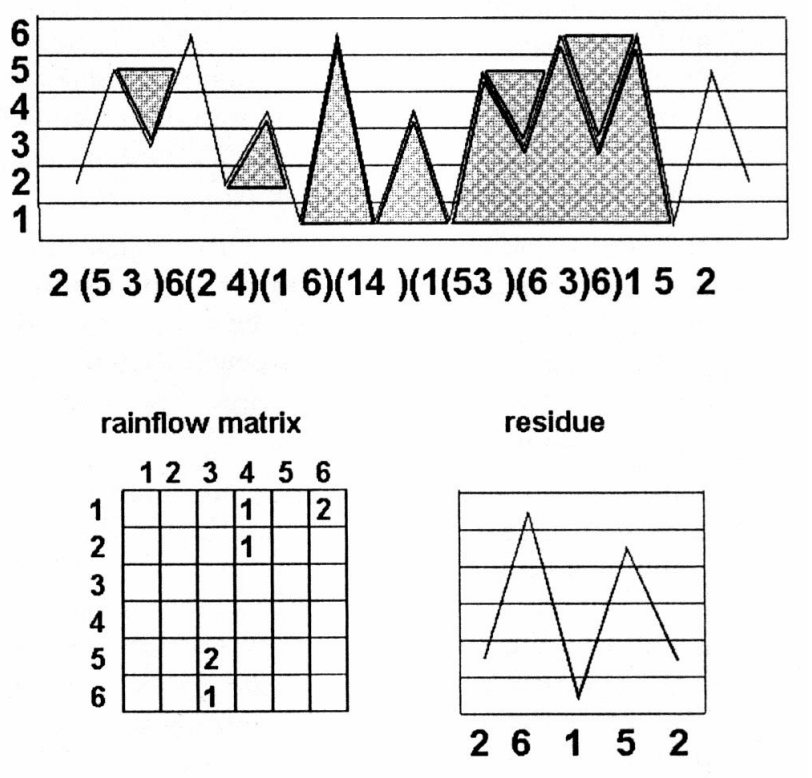

Fig. 15: The 4-point algorithm

Vpliv geometrije na utrujenostne poškodbe

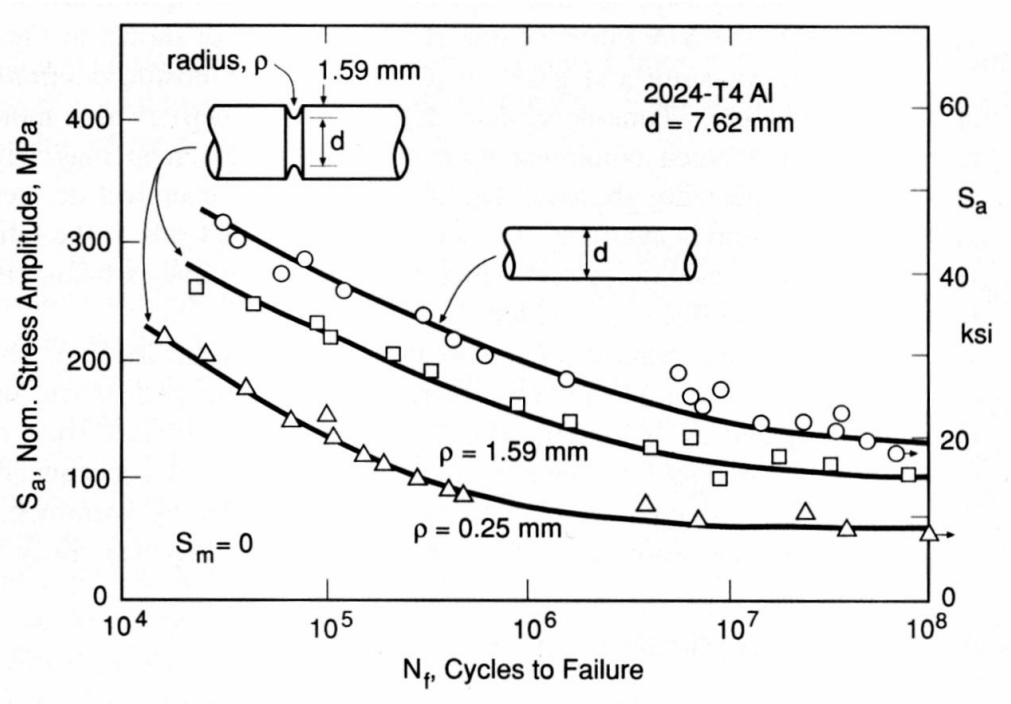

Figure 9.26 Effects of notches having $k_t = 1.6$ and 3.1 on rotating bending S-N curves of an aluminum alloy. (Adapted from [MacGregor 52].)

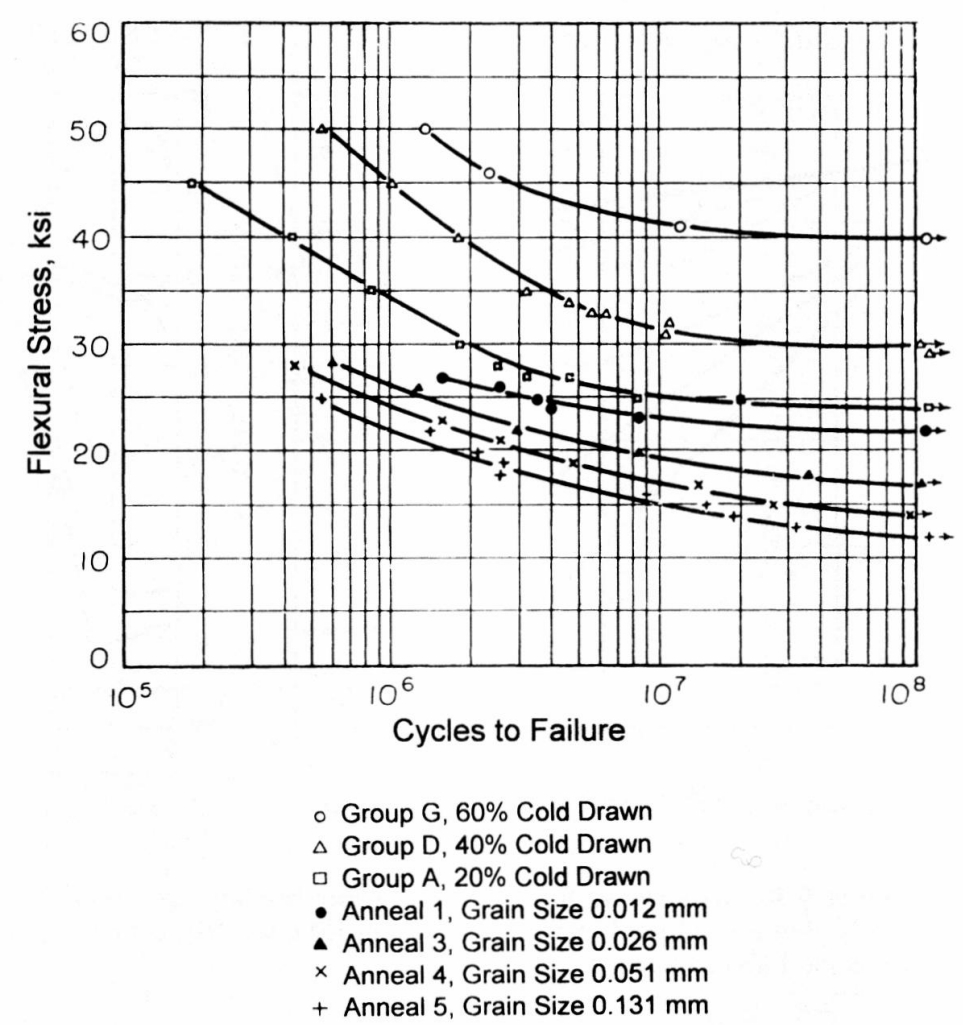

Figure 9.29 Influence of grain size and cold work on rotating bending *S-N* curves for 70Cu-30Zn brass. (From [Sinclair 52]; used with permission.)

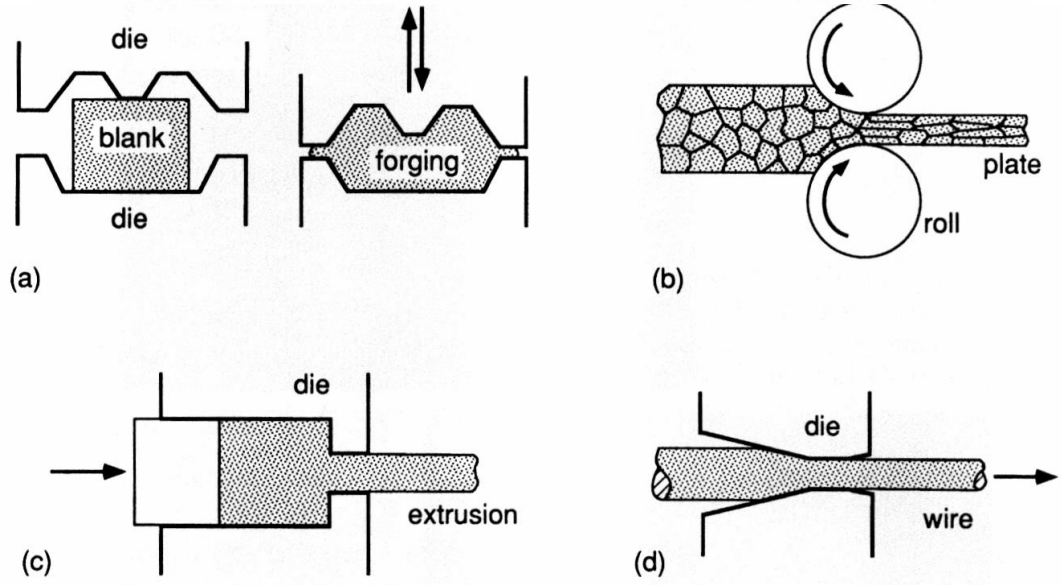

Figure 3.1 Some methods of forming metals into useful shapes: (a) forging employs compression or hammering; other methods include (b) rolling, (c) extrusion, and (d) drawing.

Vpliv koncentracij napetosti na utrujenostne poškodbe

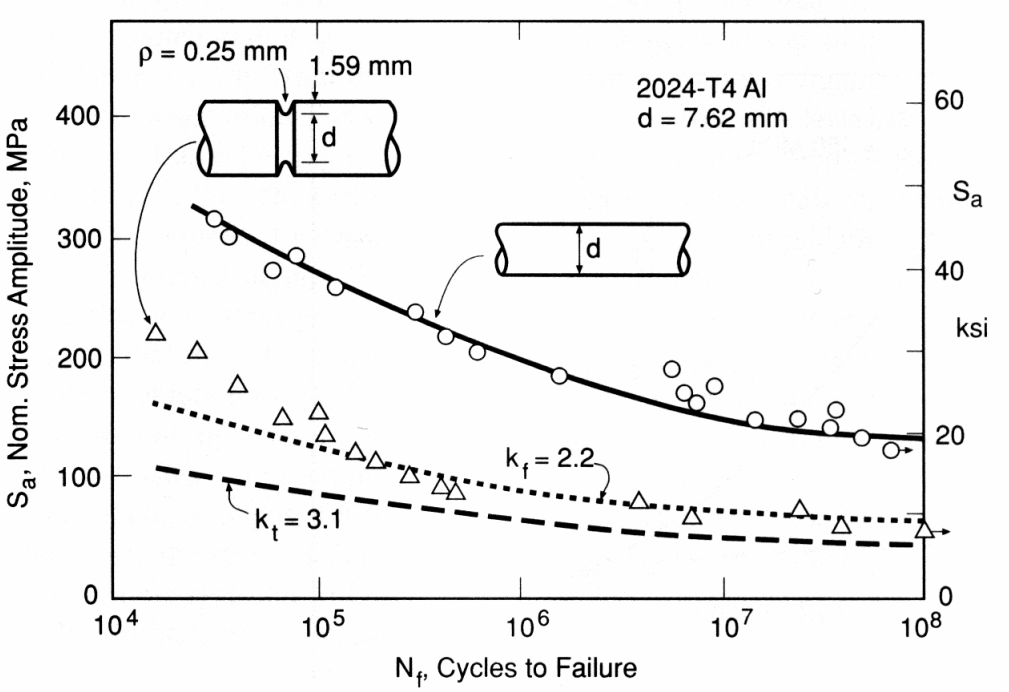

Figure 10.1 Effect of a notch on the rotating bending *S-N* behavior of an aluminum alloy, and comparisons with strength reductions using k_t and k_f. (Data from [MacGregor 52].)

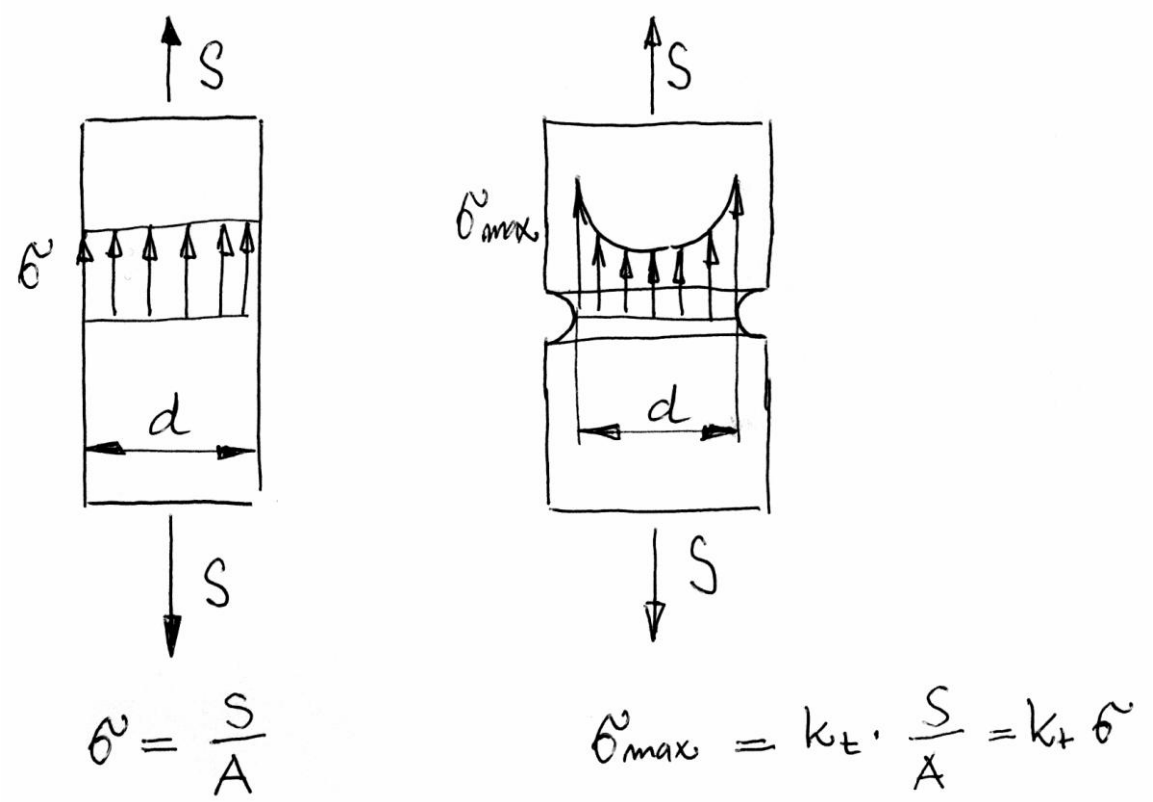

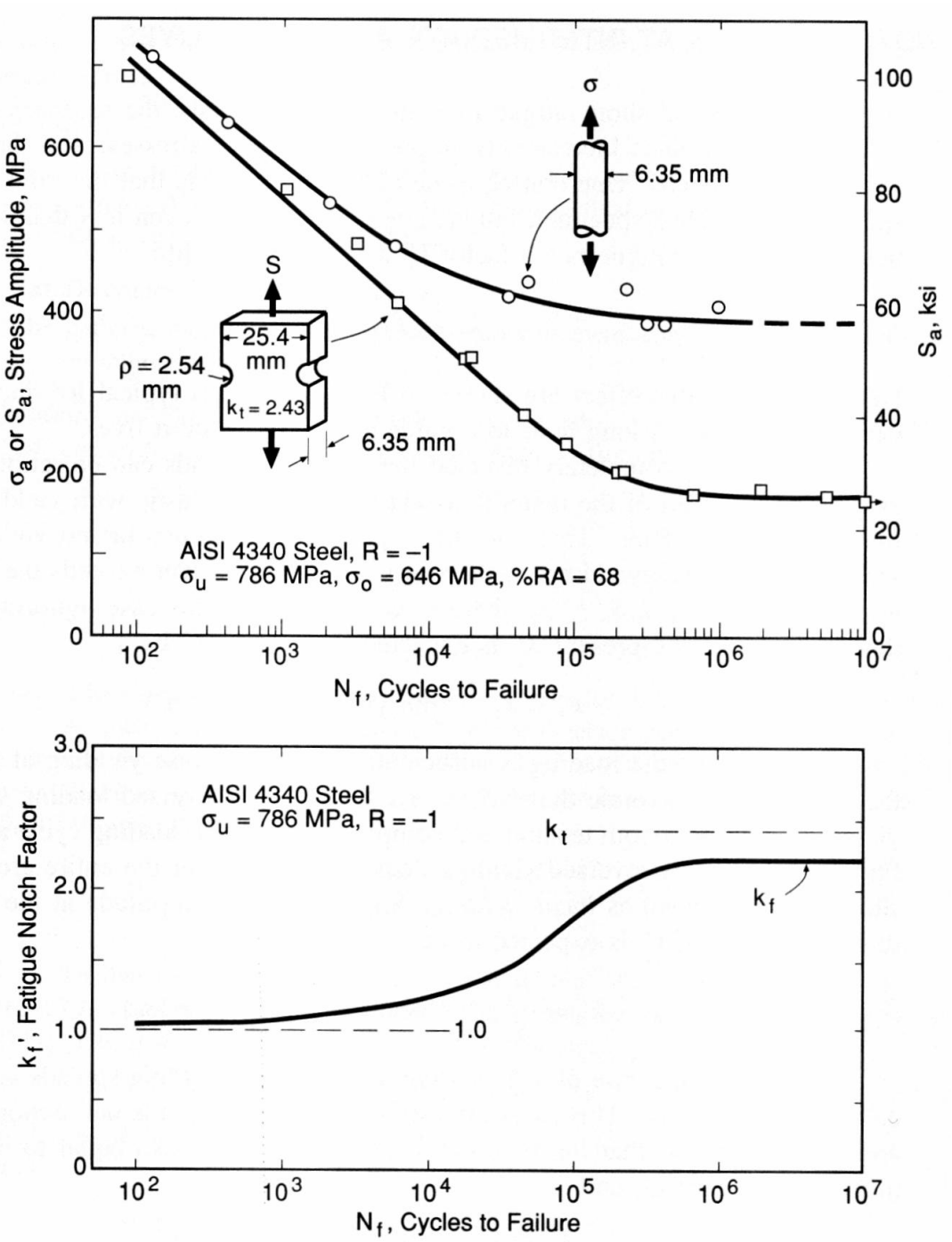

Figure 10.8 Test data for a ductile metal illustrating variation of the fatigue notch factor with life. The *S-N* data above are used to obtain $k_f' = \sigma_a/S_a$ below. The notches are half-circular cutouts. Nominal stress S is defined based on the net area as in Fig. A.8(b).

Vzroki za pojav koncentracij napetosti

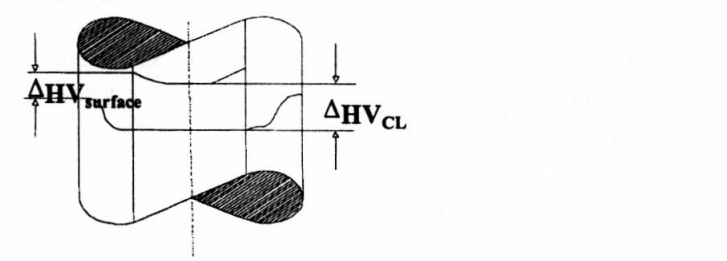

Fig. 20: Hardness profile in tempered or quenches steel

Fig. 21: Stress distribution in high strength steel due to non-metallic inclusions

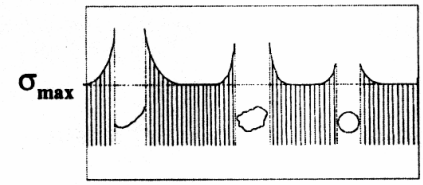

Fig. 22: Stress distribution in graphitic cast iron due to the morphology of the graphite

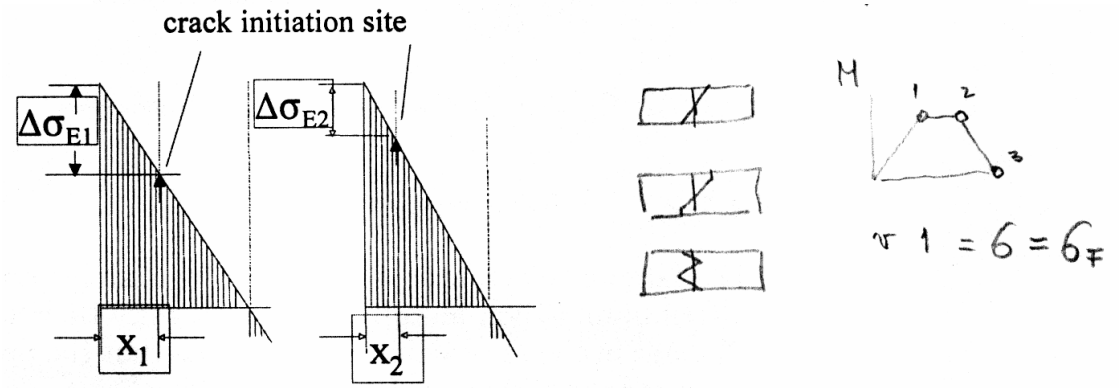

Fig. 23: Different prestresses at the inner layer after surface treatment.

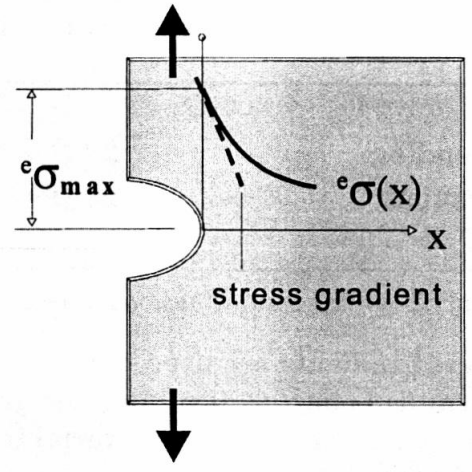

Fig. 24: Definition of stress gradient.

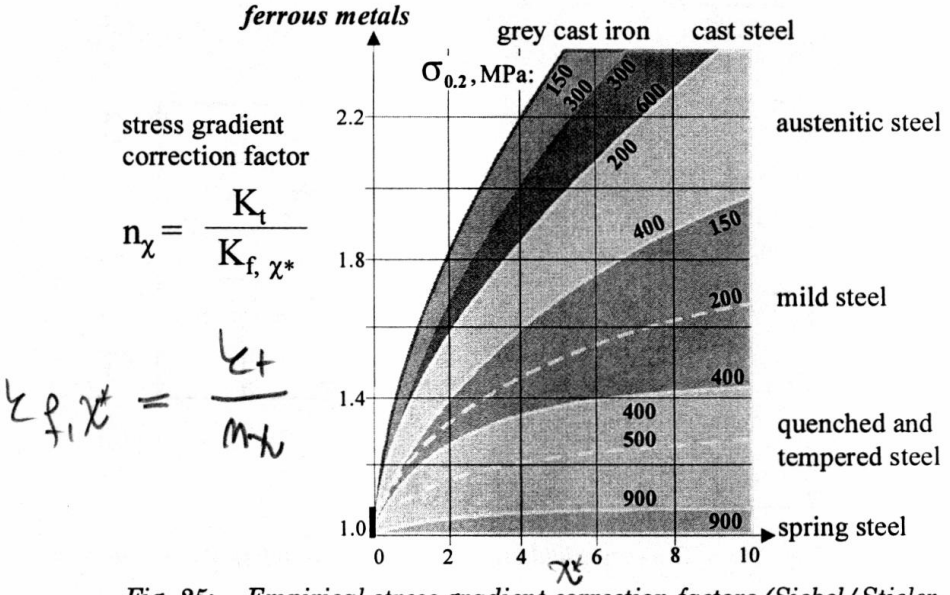

Fig. 25: Empirical stress gradient correction factors (Siebel/Stieler 1955).

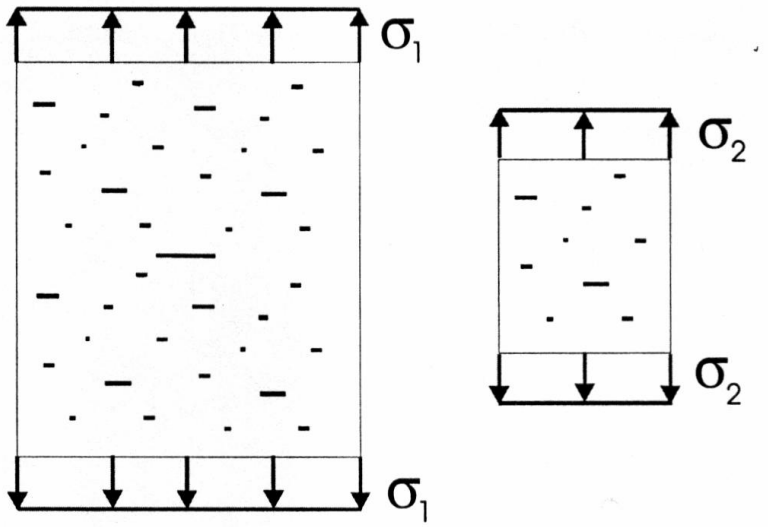

Fig. 26: The statistical size effect occurs if defect size is not constant.

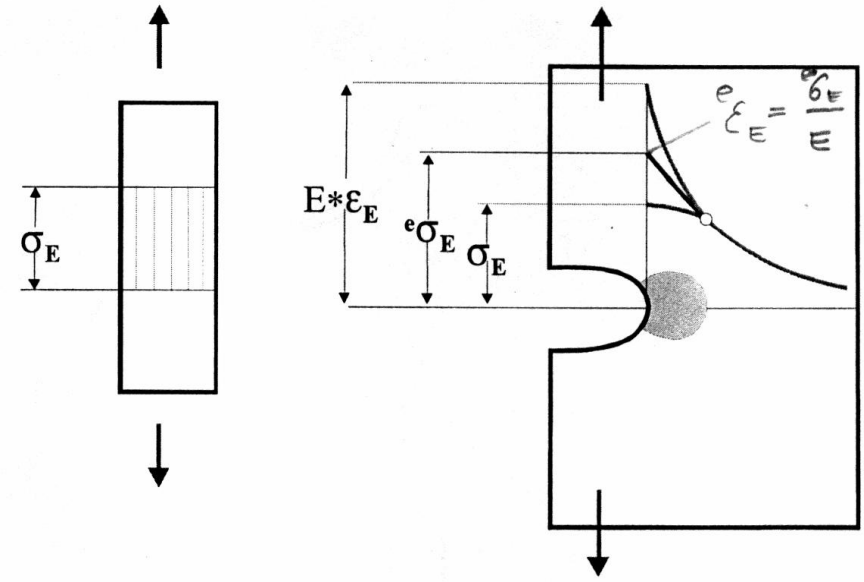

Fig. 27: Effect of macroscopic yielding on endurance limit

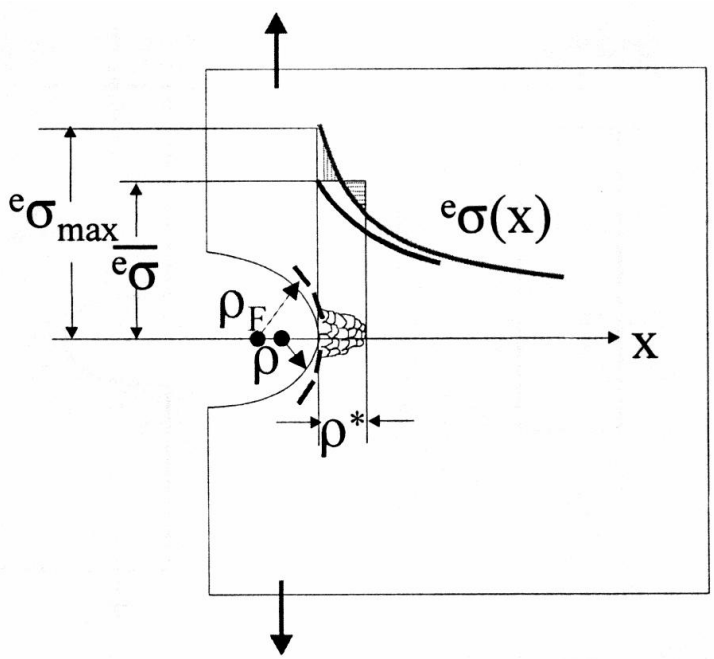

Fig. 28: Neuber's approach to micro-yielding

Vpliv hrapavosti površine na utrujenostne poškodbe

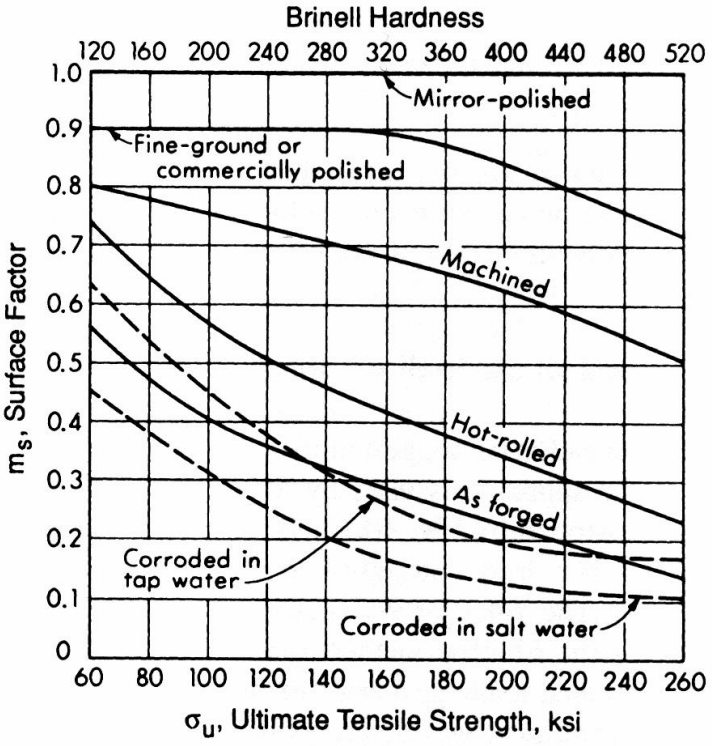

Figure 10.14 Effect of various surface finishes on the fatigue limit of steel. Values are plotted of m_s, the ratio of the fatigue limit to that for polished specimens. (Adapted from R. C. Juvinall, *Stress, Strain, and Strength*, 1967; [Juvinall 67] p. 234; reproduced with permission of the McGraw-Hill Companies.)

Vpliv velikosti prereza na utrujenostne poškodbe

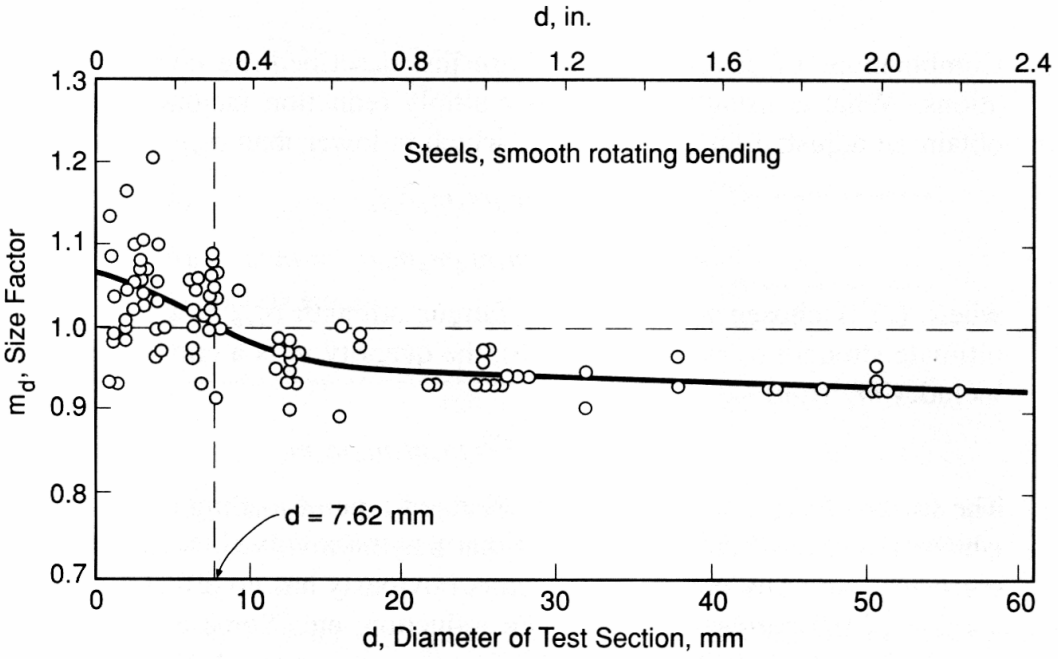

Figure 10.13 Effect of size on the fatigue limit of smoothly polished specimens of steels tested in rotating bending. Values are plotted of m_d, the ratio of the fatigue limit to that for the frequently used 7.62 mm (0.3 in.) specimen diameter. (Data from [Heywood 62] p. 23.)